Journal of Constructional Steel Research 148 (2018) 351–360

Contents lists available at ScienceDirect

Journal of Constructional Steel Research

Experimental study of Pipe-Fuse Damper for passive energy dissipation in structures

Reza Aghlara [a], Mahmood Md. Tahir [b,*], Azlan Bin Adnan [a]

[a] Faculty of Civil Engineering, Universiti Teknologi Malaysia, 81310 Johor Bahru, Johor, Malaysia
[b] Institute for Smart Infrastructure & Innovative Construction (ISIIC), Faculty of Civil Engineering, Universiti Teknologi Malaysia, 81310 Johor Bahru, Johor, Malaysia

ARTICLE INFO

Article history:
Received 6 February 2018
Received in revised form 21 May 2018
Accepted 2 June 2018
Available online xxxx

Keywords:
Passive control
Metallic yield damper
Earthquake energy dissipation
Fuse Damper (FD)
Pipe-Fuse Damper (PFD)

ABSTRACT

This study presents a novel passive metallic damper, Pipe-Fuse Damper (PFD), to improve the seismic response of structures with dissipation of the earthquake energy. The Fuse Damper (FD) was recently introduced by using steel bars as fuses, Bar-Fuse Damper (BFD), and its performance was evaluated experimentally. The Fuse Damper (FD) is built using common cross-sections found in engineering structures, such as square hollow sections (SHS) and U-shaped sections as well as metal sheets. As a special feature, the Fuse Damper (FD) uses replaceable components as an energy-absorber part with both flexural and tensile energy dissipating mechanisms. In this study, the Fuse Damper (FD) was evaluated with components of steel pipes experimentally and numerically. To assess the individual performance of this damper, the Pipe-Fuse Damper (PFD), a series of monotonic and cyclic experiments were conducted on real-scale specimens. The studied parameters for this replaceable element in the experiments were the number of pipes and their diameter, length, and thickness. The results indicate that, in addition to demonstrating a stable hysteretic behaviour and considerable energy dissipation within an appropriate displacement reversal, the proposed damper offers the easy replacement of pipe components after each failure. Moreover, the Pipe-Fuse Damper (PFD) showed less pinching effects on its hysteresis and a higher energy dissipation compared to the Bar-Fuse Damper (BFD) under the same conditions.

1. Introduction

Among passive control systems, metallic yield dampers are economical and do not require advanced production technologies, and they can also effectively improve seismic structural responses [1]. Moreover, these kind of dampers can be simply modelled mathematically and numerically, which is highly important in the development, design, and prediction of their behaviour. Energy dissipation in this type of damper occurs in the form of plastic deformation of the energy-absorber members through different flexural, shear, and torsional mechanisms. These dampers were first manufactured in Japan and New Zealand almost 50 years ago. In Japan, the slitted wall and the damping strips for the partition walls were employed by Muto and Guerrero in several structures to dissipate energy [2, 3]. Experimental research was conducted by Kelly and Skinner on energy absorption devices such as torsional beams, u-strips, and flexural beams in New Zealand [4, 5].

The Added Damping and Stiffness (ADAS) and the Steel Slitted Damper (SSD) are among the most popular metallic yield dampers, which have practical applications and are employed as passive control systems in a number of structures in developed countries [6, 7]. The ADAS is composed of a set of energy-absorber X-shaped or triangular steel sheets installed between the Chevron braces and its respective beam frame to dissipate the energy transferred to the structure through the flexural mechanism of the sheets. With a similar installation procedure to the ADAS, the SSD damper includes one or more slitted sheets that dissipate energy through in-plane plastic deformation and the flexural shear mechanism. These two dampers are specifically designed for Chevron braces and they cannot be installed in diagonal braces. A new damper, the Cast-Steel Yielding Brace (CSYB), performs similarly to the ADAS damper, with the exception of its constituting material which is made of cast steel, and it can be installed in diagonal braces [8]. In recent years, numerous and various innovations have been presented regarding metallic dampers by researchers, some of which are practically implemented in structures, while some of the others are still in the experimental stages [9, 10].

Since metallic dampers protect the main structural members against earthquakes by absorbing energy and directing possible destruction to their energy-absorber members, it can be claimed that they function like a fuse [11, 12]. However, this terminology mainly focuses on the protective characteristics of dampers and is less associated with the replaceable characteristic of fuses. Therefore, a new metallic damper, the Fuse Damper (FD), was designed to offer the capability of energy

* Corresponding author.
E-mail addresses: areza24@live.utm.my, (R. Aghlara), mahmoodtahir@utm.my (M.M. Tahir).

https://doi.org/10.1016/j.jcsr.2018.06.004
0143-974X/

dissipation with flexural and tensile mechanisms through appropriate replaceable components (fuses), e.g. steel bars or pipes. The longitudinal energy absorber members in the FD can be produced from any material with any cross-sectional shape and geometrical dimensions if they can appropriately dissipate energy. The characteristics and behaviour of the proposed damper can be controlled through five factors related to its fuses: the material and shape of the components; and the number, length, and size of the components. The rigid body of the damper is designed such that the total applied displacement can be transferred to the fuses, which consequently causes their plastic deformation. The experimental and numerical study of the Fuse-Damper (FD) with steel Bars (BFD) was previously conducted and presented recently [13]. In the present study, simple steel pipes were used as the energy-absorber fuses in the FD.

In literature related to the structural control, almost the same framework of methodology can be found to evaluate newly proposed devices [14–20]. Following this common procedure, the current study evaluates characteristics of the Pipe-Fuse Damper (PFD) individually, while its effect on seismic structural behaviour will be examined in future works. The outline of this study is summarized as the following: the results of conducted experiments are presented to evaluate the hysteretic behaviour of the proposed damper. According to the results, two important properties of metallic dampers, namely the capacity of the dissipated energy, and the equivalent viscous damping ratio are calculated and presented. To verify the experimental results and also to conduct a parametric study, the PFD was modelled and nonlinearly analysed using general finite element software ANSYS. Based on the results of the parametric studies, the formulas for mechanical properties of the PFD were derived which can be useful for initial design of the damper. Moreover, the characteristics of FD with steel bar (BFD) and with steel pipe (PFD) are compared to assess the influence of different sacrificial elements to the proposed damper.

2. Pipe-Fuse Damper (PFD)

The proposed damper is a metallic yield damper that uses steel pipes as replaceable fuses to absorb energy. All the geometric details of the PFD are presented in Fig. 1. As shown in the figure, the PFD is composed of three main parts that includes an outer part, an inner part, and a fuse part. The inner and outer parts are two rigid parts of the PFD, which interconnect to each other by the flexible fuse part.

The outer part has three main components: one hollow square steel profile, two reinforced steel plates, and one end steel-plate. For passing of the steel pipes through the outer part, some suitable holes are embedded in two opposite sides of the hollow square profile. Two perforated reinforced plates are fully welded to the profile from the outside to prevent the profile's body from local buckling. The end steel-plate in the outer part is devised to connect the PFD to the brace that has the similar plate at its end through appropriate bolts.

The inner part of the PFD also has three main components: two channel profiles, one perforated steel plate, and one end steel-plate. As shown in Fig. 1, the perforated steel plate connects the two channels to each other symmetrically along with the end plate at one end of the three components. The holes in the perforated plate are there to pass the steel pipes and the end plate has the same function as the one in the outer part. All the components of the inner parts, like those for the outer part, are properly welded to each other to form a rigid part to ensure negligible deformation under the axial loading of the braces. It is needless to say that the holes for the passing of the pipes are drilled in a similar pattern for both the outer and inner parts.

The fuse part consists of threaded steel pipes that interconnect the outer and inner parts to each other conveniently. The easy replacement capability of the steel pipes (fuses) in the case of failure is the key feature of the proposed damper. The compressive and tensile axial forces in the braces induced by earthquakes, produce back and forth motions of the inner part inside the outer part. In result, these motions cause consecutive plastic bending deformations at the middle of the steel pipes in two opposite directions. In essence, a portion of input energy of an earthquake into a structure is dissipated by the flexural plastic deformation of the steel pipes to reduce the plastic deformation demands in primary structural elements.

The PFD can be installed on different types of conventional braces at favourite locations with fewer limitations in comparison with the other metallic dampers. For example, the PFDs are installed at the middle of the diagonal and Chevron braces in a frame, as shown in Fig. 2. Furthermore, the proposed damper can be utilized for seismic retrofitting purpose of steel/concrete structures in the form of an arrangement suggested by Lee, similar to the configuration scheme of the knee braces [10].

As noted earlier, some part of the seismic energy that exerted on the system can be dissipated through the deformation of the plastic pipes in the damper. Thus, the rest of members in the frame are protected through a reduction in the plastic deformation. The energy absorption mechanism in the PFD is largely dependent on the amount of motion. In other words, for small motions the mechanism is the flexural type, while for large motions the mechanism is the flexural-tensile type. This variation in the mechanisms can be considered as one of the strengths of the PFD because it increases the secondary strength and stiffness of the damper as will be observed from results in the next sections.

3. Experimental study

To study the behaviour of the proposed damper and to assess its mechanical properties, several component tests were conducted on four full-scale PFDs. The influence of four key parameters has been evaluated on the performance of the damper, namely the number, diameter,

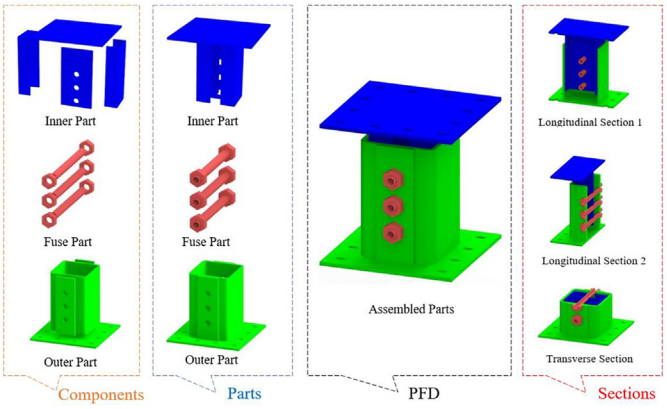

Fig. 1. Geometric illustration of Pipe-Fuse Damper (PFD).

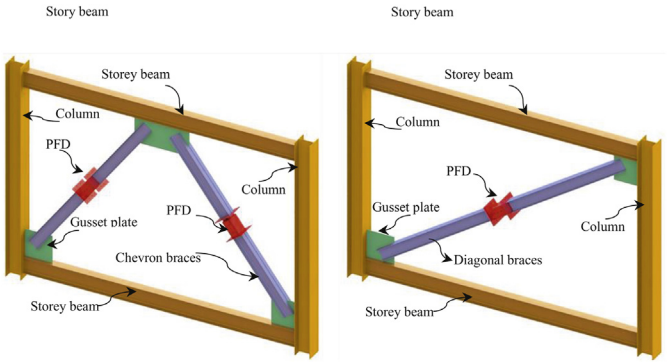

Fig. 2. Two proposed placements for Pipe-Fuse Damper (PFD).

Table 1
Dimension of PFD components.

Parts	Components	QTY	ID	Length (mm)	Width (mm)	Depth (mm)	Flange Width (mm)	Thickness (mm)	Diameter (mm)	Description
Outer part	Square Tube (BSI)	1	1	300	200	200	–	6	–	6 Holes 22/28 mm
	Added Plate (outside)	2	2	300	100	–	–	10	–	3 Holes 22/28 mm
	Connection Plate	1	4	350	350	–	–	10	–	12 Slots for M12
Inner part	Connection Plate	1	6	350	350	–	–	10	–	12 Slots for M12
	RSC Channels (BSI)	2	8	300	–	127	64	6.4	–	
	Middle Plate	1	9	300	160	–	–	10	–	3 Holes 22/28 mm
Fuse part	Seamless steel pipes	–	11	280	–	–	–	2.6, 3.9, 3.8	21, 27	35 mm Threaded Ends

Table 2
List of tests and specimens' specifications.

Specimens	Phase	Pipes				Tests	
		Diameter (mm)	Thickness (mm)	Length[a] (mm)	Number	Monotonic	Cyclic
1Pipe21(3)-188	1	21.2	2.42	188	1	x	x
2Pipe21(3)-188	1	21.2	2.42	188	2	x	x
3Pipe21(3)-188	1	21.2	2.42	188	3	x	x
1Pipe21(3)-158	2	21.4	2.65	158	1	x	x
2Pipe21(3)-158	2	21.4	2.65	158	2		x
1Pipe21(3)-188	2	21.4	2.65	188	1	x	x
2Pipe21(3)-188	2	21.4	2.65	188	2		x
1Pipe21(4)-158	2	21.4	3.95	158	1	x	x
2Pipe21(4)-158	2	21.4	3.95	158	2		x
1Pipe21(4)-188	2	21.4	3.95	188	1	x	x
2Pipe21(4)-188	2	21.4	3.95	188	2		x
1Pipe27(4)-168	2	26.7	3.8	168	1	x	x
2Pipe27(4)-168	2	26.7	3.8	168	2		x
1Pipe27(4)-188	2	26.7	3.8	188	1	x	x
2Pipe27(4)-188	2	26.7	3.8	188	2		x

[a] Length of bending (free inside distance of Square Tube).

length, and thickness of the steel pipes. A number of monotonic tests were conducted to determine some important properties, such as displacements and strengths at the yielding and ultimate points of the damper. A series of cyclic experiments were also conducted to estimate important values, such as the strength and stiffness; the equivalent viscous damping ratio; and the amount of dissipated energy under specific loading protocols.

3.1. Specimens and material properties

Two PFDs which had different pipe diameters of 21 and 27 mm, were developed in such a way that they remained intact for multiple testing with little plastic deformation of the inner and outer parts. As previously mentioned, the force subjected to the damper was endured by the replaceable steel pipes and the outer and inner parts of damper are responsible for transferring the loads rigidly. To perform several experiments, therefore, only the failed pipes from the previous tests were removed and replaced by new pipes, while the outer and inner parts for the same pipe's diameter were used for the various tests. The ease of replacing the damaged pipes can prove the proposed damper's fuse-like performance. Table 1 shows the list of the components used in the PFD and their geometric dimensions.

To facilitate codification of the specimens, a specific procedure was defined as [No. 1][Element][No. 2][No. 3]- [No. 4]. “No. 1” represents the number of fuses used. “Element” indicates the type of fuse used, which are pipes in this study. Then, “No. 2” and “No. 3” represent the diameter and thickness of pipes in millimetres. Whereas, “No. 4” shows the bending length of the pipes or the inner dimensions of the hollow square tube in millimetres. Table 2 shows the list of tested specimens, their geometry, and the type of tests performed on specimens.

To achieve the material properties of the steel pipes used in the dampers, a total of six tensile tests were conducted on the pipe samples according to the ASTM code [21]. The mean values of the properties for different pipes diameters are presented in Table 3.

3.2. Tests setup and loading protocol

The INSTRON machine was utilized to perform the experiments in this study. Fig. 3(a) shows the schematic of the experimental setup for the proposed damper. Two types of device-controller software, which are known as BlueHill and WaveMaker, were used for monotonic and quasi-static cyclic tests, respectively. This testing machine provides loading, unloading, and recording of data (force and displacement) through an interface device connected to a desktop computer. Fig. 3 (b) depicts the specimen 3Pipe21(3)-188 installed in the INSTRON before the cyclic test commenced.

To derive a displacement load reversal, the FEMA461 guideline was used for cyclic experiments in this study [22]. The target displacement required for calculating this loading history was selected based on results of the monotonic tests. The displacement load was divided into 10 steps with specified displacement amplitudes calculated in a specific way that was laid down in the guideline based on the selected target displacement. In the case, where the specimen did not fail after 20 cycles, the next steps included one cycle with a 1.3-fold last displacement amplitude, where this process continued until the complete

Table 3
Material properties of pipes.

Pipe diameter (mm)	Thickness (mm)	Modulus of elasticity (GPa)	Yield stress (MPa)	Ultimate stress (MPa)	Elongation (%)
21 (21.4)	3 (2.65)	213.5	326.8	455.8	36
21 (21.4)	4 (3.95)	236.3	342.7	491.7	34
27 (26.7)	4 (3.80)	216	340.2	475.2	46

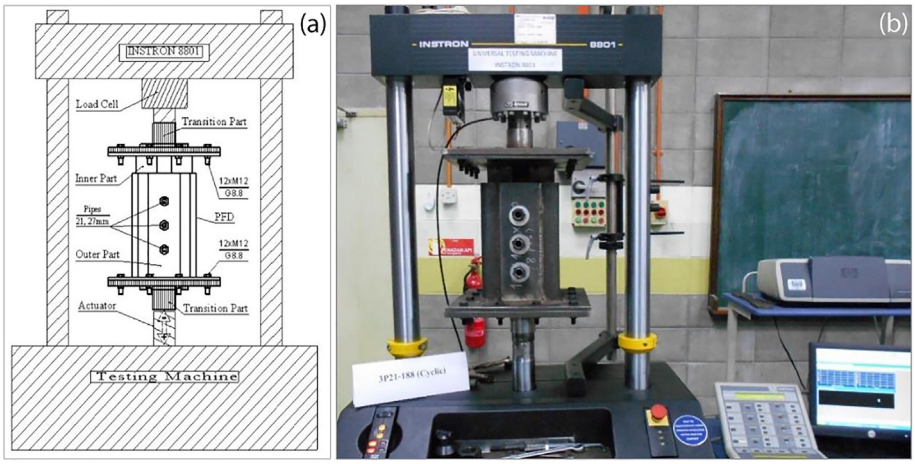

Fig. 3. Tests setup: a) schematic sketch, b) photo of 3Pipe21(3)-188 mounted on INSTRON.

failure of the pipes. Fig. 4 shows the employed load protocol in the conducted cyclic tests.

3.3. Experimental results and discussions

A series of quasi-static cyclic tests were performed on the full-scale Fuse Damper (FD) with replaceable steel pipes. The downward and upward forces were subjected to the outer part of the PFD at a rate of 10 mm/min using the displacement control method. The obtained force-displacement hysteresis for four PFDs are shown in Fig. 5. According to the diagrams, the response of the dampers under cyclic loads was in the form of a regular, similar, and stable pattern. In all the experiments, the PFDs showed acceptable ductility and energy absorption characteristics so that a sudden drop in the strength and stiffness was not observed in the hysteresis loops within an appropriate displacement domain.

In all cases, the results showed that the strength and elastic stiffness responses of the samples with two pipes were two times stronger than the response of corresponding samples with one pipe. This feature reflects the important fact that, in addition to the three control factors, i.e. the pipe length, diameter, and thickness in the PFD, the number of pipes can be used as a control factor as well.

Both the monotonic and cyclic responses of specimen 1Pipe27(4)-168 were shown in Fig. 5(b). A comparison of the two responses shows that the trend of strength enhancement is similar for the specimen in the two tests. However, a slight degradation was achieved in the cyclic strength due to low-cycle fatigue life of the steel material. Considering the ultimate displacement of 20 mm from the monotonic test and the target displacement of 10 mm in the cyclic test, it can be argued that the PFD can have a stable hysteretic behaviour within a range equal to or less than 50% of the monotonic ultimate displacement.

The displacement in the yield point was less than 2.5 mm in both monotonic and cyclic responses associated with a smooth transition from an elastic to a plastic phase. Also, according to the hysteresis of the specimens, a sudden increase in the strength and stiffness is

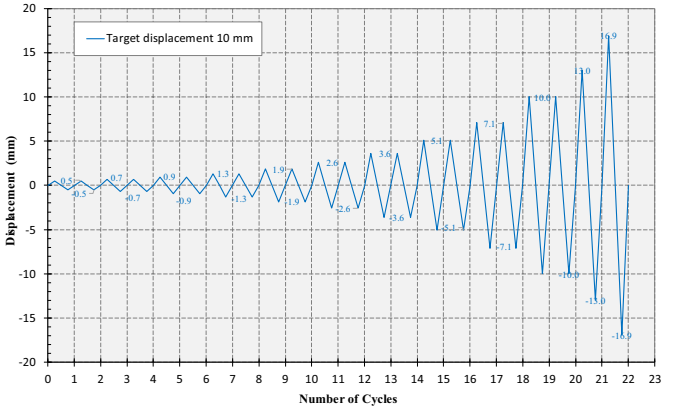

Fig. 4. Applied displacement load protocol.

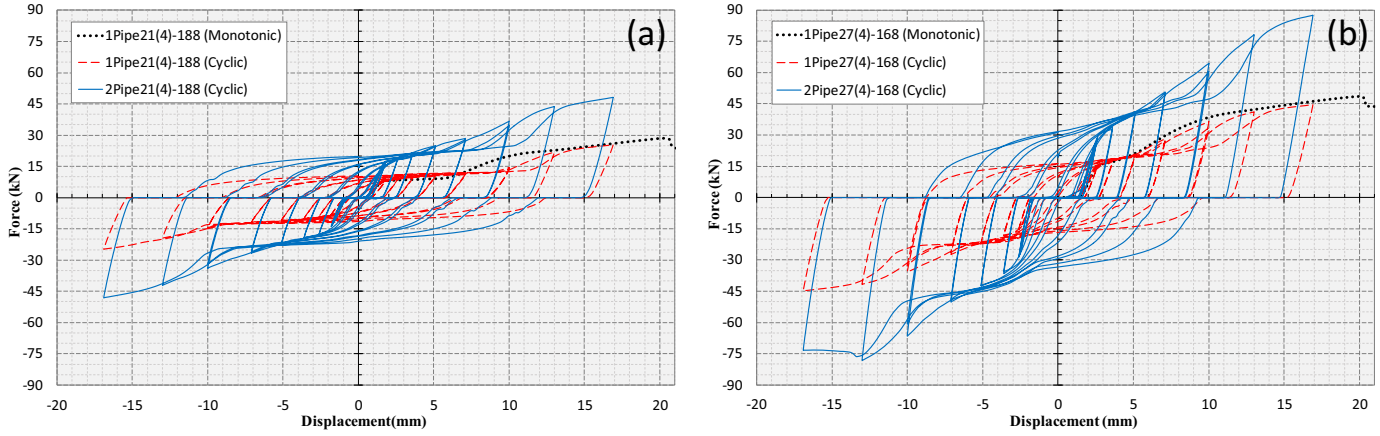

Fig. 5. Experimental monotonic and cyclic response of the specimens: a) 1/2Pipe21(4)-188, b) 1/2Pipe27(4)-168.

Table 4
Mechanical properties from cyclic tests and calculated key parameters.

Specimens	P (kN)						Nc	Dis./L	K_{eff}^{avg}	Cum. energy	ξ_{eq}^{avg}
	@ + displacements			@ - displacements							
	+10 mm	+13 mm	+16.90 mm	−10 mm	−13 mm	−16.90 mm			(kN/mm)	(J)	
1P21(2.6)-188	14.60	14.42	15.02	−14.90	−16.43	−15.20	22	0.053	2.06	2316	0.47
2P21(2.6)-188	30.63	23.65	23.95	−31.43	−22.92	−24.96	22	0.053	5.27	4089	0.55
1P21(2.6)-158	20.89	21.74	11.96	−21.07	−17.86	−10.81	22	0.060	3.87	2449	0.48
2P21(2.6)-158	42.11	43.55	24.89	−42.33	−35.49	−21.77	22	0.060	7.04	5554	0.50
1P21(3.9)-188	14.52	21.87	25.40	−14.81	−19.31	−24.58	22	0.053	2.51	3193	0.50
2P21(3.9)-188	36.64	43.78	48.19	−33.89	−42.09	−48.10	22	0.053	4.52	6147	0.43
1P21(3.9)-158	27.56	28.50	13.77	−27.74	−19.31	−14.05	22	0.060	4.52	3368	0.49
2P21(3.9)-158	54.94	56.35	28.60	−55.29	−41.81	−27.91	22	0.060	8.50	7176	0.50
1P27(3.8)-188	32.79	36.04	38.91	−29.20	−34.45	−38.41	22	0.053	3.64	4512	0.38
2P27(3.8)-188	62.07	70.00	77.05	−55.50	−63.87	−73.57	22	0.053	7.13	9101	0.46
1P27(3.8)-168	36.22	41.04	44.53	−35.80	−41.62	−44.83	22	0.060	2.62	4883	0.37
2P27(3.8)-168	64.35	78.05	87.43	−66.52	−78.26	−73.33	22	0.060	4.86	9466	0.39

noticeable from load cycle seven and onwards, which could be due to a transformation of the energy dissipating mechanism from flexural to tensile. Important properties, such as the maximum force (P) in opposite directions for the last three cycles, the number of cycles (Nc) sustained by the PFD, and the ratio of pipe displacement to the pipe bending length (Dis./L), are presented in Table 4. As it is seen in this table, all specimens not only sustained 20 cycles at the target displacement, but they also endured two more cycles up to 17 mm. This shows there is an appropriate safety margin beyond the selected target displacement for a reliable performance of the PFD.

Another important factor for the PFD is the ratio of the target displacement to the pipe bending length that was selected less than 6% as presented in Table 4, estimated based on experiences from preliminary tests. This ratio is directly associated with the number of endured cycles, and the selection of a value below the mentioned margin could guarantee the damper performance without compromising a considerable strength and stiffness. Having the value of this ratio from one hand and the required drift ratio for a frame from the other hand, the pipe length of the PFD can be easily calculated by geometric relationships. Fig. 6 shows three photos of failed pipes taken after the cyclic tests of the related specimens. As can be seen, the failures occurred in the middle of the pipes through the mechanism of necking. Damaged pipes are easily replaced with new pipes for further testing.

Since the performance of metallic dampers is dependent on the displacement rather than on force velocity, their damping is defined as the equivalent viscous damping ratio according to Eq. 1, where E_D denotes the energy dissipated in a hysteresis loop and covers the area enclosed in the loop, and E_s is the strain energy in an elastic spring with an equivalent stiffness (K_{eff}) and displacement (D) that is equal to $0.5K_{eff}.D^2$ [13]. The effective stiffness can be calculated based on the maximum force-displacement values for a cycle in opposite directions through Eq. 2.

$$\xi_{eq} = \frac{1}{4\pi}\frac{E_D}{E_S} = \frac{1}{2\pi}\frac{E_D}{K_{eff}D^2} \quad (1)$$

$$K_{eff} = \frac{|P_{max}| - |P_{min}|}{|D_{max}| - |D_{min}|} \quad (2)$$

To determine the stiffness and equivalent viscous damping ratio of each PFD, these values were initially calculated for each cycle of the related hysteresis using the presented equations and then averages of the values were computed regarding the total number of cycles (Nc) for each device. The mean stiffness and equivalent damping ratio of the tested PFDs are listed in Table 4. Variations of the damping ratios with the pipe diameters show that these parameters are inversely correlated to each other when the pipes have the same thickness. Whereas, under the same circumstance, the effective stiffness has a proportional relation with the pipe diameter. The overall average of the equivalent damping ratio is about 0.46 for the PFD, and this amount complies with the ranges of damping ratios that are classified based on the mechanisms of energy dissipation, presented in another study [23].

Fig. 7 shows the changes in the equivalent viscous ratio against the effective stiffness for the different specimens. In this figure, each point presents the damping ratio and the equivalent stiffness for a specific cycle of a specimen in the experiment. According to this figure, any increase in the pipe diameter leads to an increase in the equivalent stiffness, but this also reduces the mean damping ratio. Moreover, any length decrease in the pipe will increase the equivalent stiffness, but the damping value remains almost constant. By adding the number of load cycles (displacement increasing), the damping ratio increases directly. Hence, it can be concluded that any increase in displacement will reduce the equivalent stiffness. In other words, changes in the equivalent damping ratio are inversely correlated to equivalent stiffness. Obtaining a range from 25 to 80% for equivalent damping ratio shows that the PFD can be used as an energy dissipating device in structures.

Fig. 8 shows the cumulative dissipated energy versus the displacements for six different specimens, where each was tested cyclically with one and two pipes. As the figure shows, the dissipated energy increases almost linearly with any increase in the displacement. Not surprisingly, the increase in the dissipated energy was insignificant in the elastic region, but significant in the plastic region. The diagrams show that the absorbed energy is directly correlated with an increase in the number, diameter and thickness of the pipes; whereas, the increased pipe length decreased the amount of energy absorbed. Considering the low weight of the pipes, the PFD can dissipate a considerable amount of energy along with an appropriate cumulative displacement. For example, the specimen 2Pipe27(4)-168, which consisted of pipes with a total weight of 1 kg, dissipated more than 9 kJ of energy and a cumulative displacement of 390 mm.

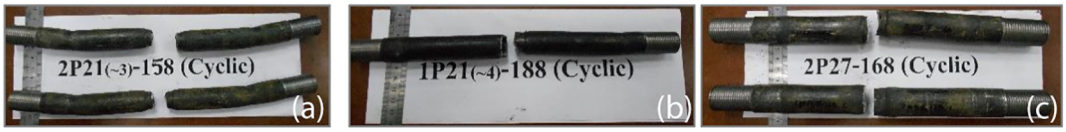

Fig. 6. Failed pipes in PFDs: a) 2Pipe21(2.6)-158, b) 1Pipe21(3.9)-188, h) 2Pipe27(3.8)-168.

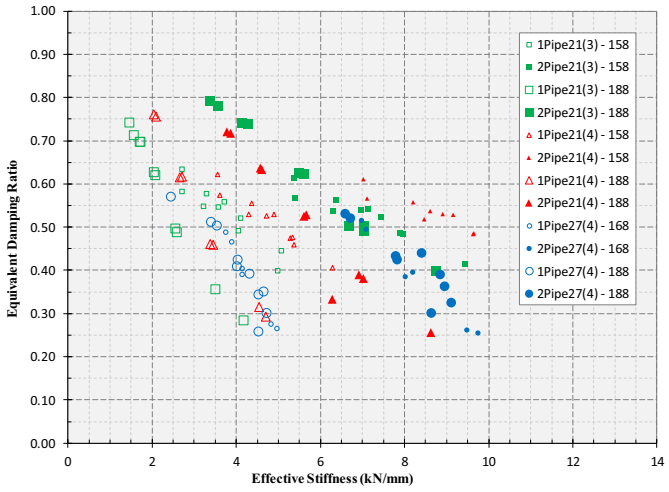

Fig. 7. Equivalent damping ratio vs. effective stiffness for PFD.

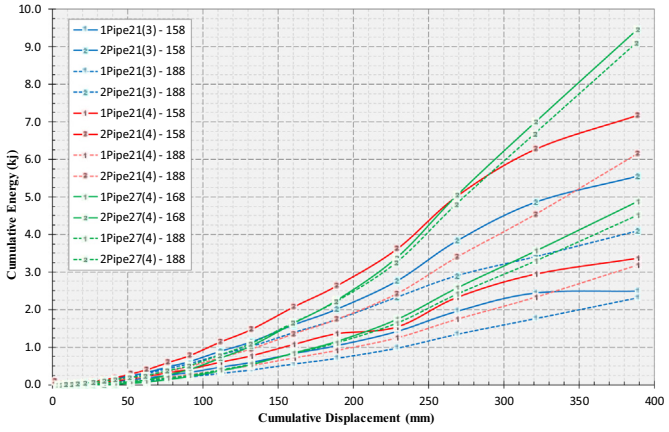

Fig. 8. Cumulative dissipated energy vs. displacements for PFDs.

4. Numerical study

For further investigation and verification of the experimental studies, the PFD was modelled and analysed non-linearly using the general finite element program ANSYS (Workbench) [14]. All the effective parts in the behaviour of the proposed damper were modelled in this software excluding the channels of the inner damper, which do not have a significant impact on the hysteretic behaviour of the PFD.

As shown in Fig. 9(a), because of two symmetrical planes perpendicular to each other in the PFD, a quarter of that was modelled and analysed to reduce the number of meshes and the cost of calculations. The model was meshed using high quality 3D solid elements. All the contact surfaces between the pipe and the inner/outer parts were defined as non-frictional due to their slight movement and negligible effect on the general behaviour, whereas the contact surface of the pipe with the nuts was defined as bonded for the ease of analysis. The geometric properties and the used material were considered with non-linear behaviour in all analyses of the models. Also, the material properties and the stress-strain relation were defined based on the results obtained from the tensile tests. The cyclic displacement load, supports, and boundary conditions were assigned to the models like the relevant specimen conditions in the experimental tests.

Fig. 9(a) shows a quarter of the model for 1Pipe27(4)-188 associated with the contour of mesh quality in the skewness format. It is recommended to keep the skewness value for solid elements less than 0.95 to achieve optimal mesh qualities. Fig. 9(b) shows the deformation contour of the half PFD under the subjected displacement of 17 mm in the last cycle. As expected, displacement occurs all through the pipe, whereas the outer part of the damper has zero displacement value.

Fig. 9(c) and (d) show counters of the equivalent Von-Mises stress and the plastic strain for half of the PFD model in the last load cycle, respectively. As can be seen in the stress contour, the replaceable member of the pipes withstands more stress compared to the other elements of the damper. This performance reflects the fact that the pipe can dissipate energy properly, which was one of the main goals in design of the PFD. The equivalent plastic strain contour shows the maximum strain location in the middle of the pipe, which exactly matches with the formation of the plastic hinge and the pipe failure in the experimental tests.

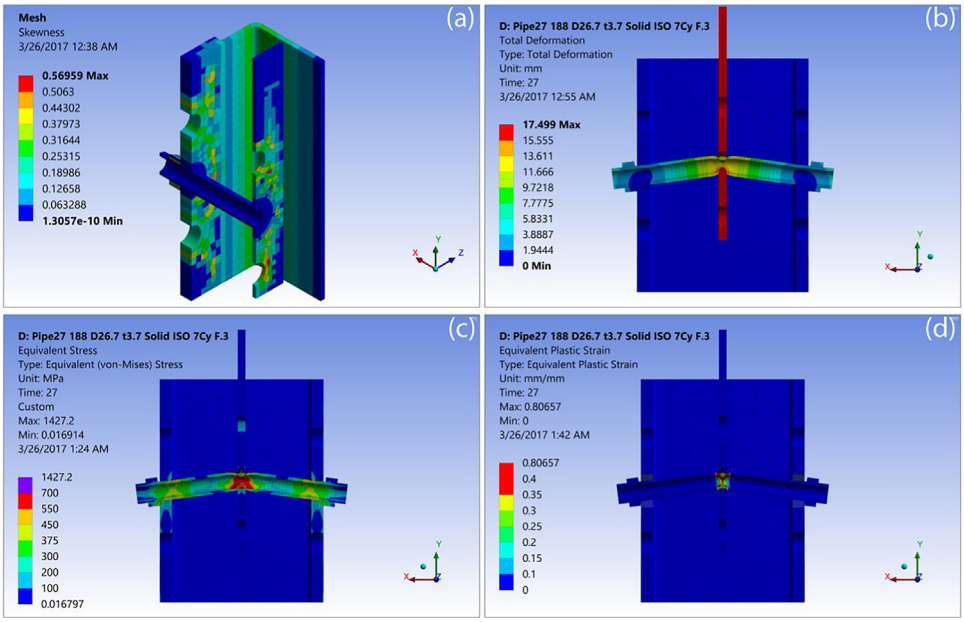

Fig. 9. Results of finite element analysis: a) mesh of BFD's quarter, b) deformation contour, c) equivalent stress contour, d) equivalent plastic strain in x-direction.

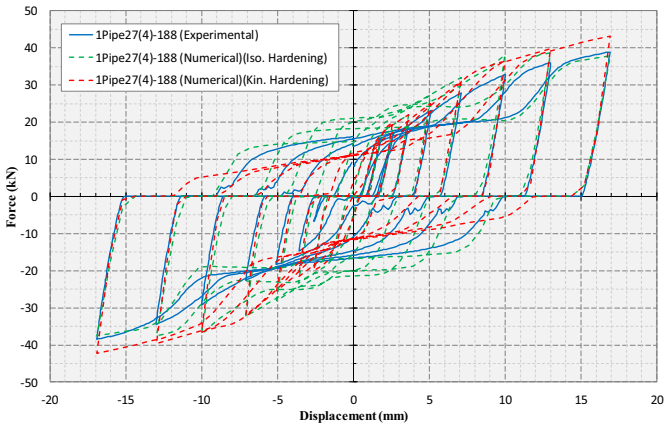

Fig. 10. Experimental and two numerical hysteresis of 1Pipe27(4)-188.

Fig. 10 shows two force-displacement hysteresis obtained from the nonlinear finite element analysis conducted on the specimen 1Pipe27(4)-188 along with the relevant hysteresis obtained from the experimental test. Two types of hardening behaviour for the material properties, isotropic and kinematic, were utilized in the numerical analyses to investigate which one better matched the experimental results. As can be seen, the results of isotropic hardening correspond to the experimental results in a finer way. Therefore, this model was selected for parametric studies.

To determine the mechanical properties of the PFD, a parametric study was conducted for 25 dampers with variation of three parameters, including the pipe diameter (D), thickness (t), and bending length (L). For this purpose, five standard pipes with different diameters and thicknesses were considered; each of which was modelled and analysed with five different lengths. To have a reliable performance, target displacements selected 5.5% of the pipe length, which was based on experiences gained from the experiments. Then, a total of 25 analyses were carried out nonlinearly for the PFD with different pipe sizes mentioned above. The results of important characteristics, such as the ultimate strength, displacement, and the stiffness in the elastic and plastic regions, are listed in Table 5. Considering the bilinear response for the PFD, maximum strength, maximum displacement, and stiffness were denoted by P_y, D_y, and K_0, respectively, in elastic phase. While, in plastic phase, these parameters were denoted by P_u, D_u, and K_p, respectively. It should be noted that the presented results are for the PFD with one pipe and it is easily extendable to a damper with several pipes.

As seen in Table 5, three key properties were also calculated for the PFD based on the results. The ultimate force to yield force ratios (P_u/P_y) (i.e. overstrength factor), have values greater than 2 for all the specimens. The ratio of yield displacement to the pipe bending length (D_y/L) has an almost constant value of about 0.01. The ratio of plastic stiffness to elastic stiffness (K_p/K_0), the last property, is almost constant and its mean is equal to 0.2.

To derive proper formulas for the mechanical properties of the PFD, the pipe was assumed to be a beam that was fixed at both ends with a concentrated force applied at its middle. The known formulas for this type of beam are $M = \frac{P.L}{8}$, $\sigma = \frac{M.Y}{I}$, and $\Delta = \frac{1}{192}\frac{P.L^3}{E.I}$, where M is the bending moment at the centre and ends, P is the concentrated load at the centre, L is the length of the beam, σ is the maximum bending stress, Y is the distance from the neutral axis to the top or bottom of the beam, whichever is the greater, E is the modulus of elasticity, and I is the moment of inertia. Assuming the same E for the materials in the pipes were used and assuming that $I = \frac{\pi (D^4 - d^4)}{64}$ is the moment of inertia for the pipes, the following dependency, namely the DL coefficients, were found by some mathematical operations for the stiffness and strength (P and K)

Table 5
Mechanical properties obtained from parametric study.

Outside diameter (D)		t[a]	d[b]	Length (L)	P_y	D_y	K_0	P_u	D_u[c]	K_p	P_u/P_y	D_y/L	Kp/K_0	[d]$D' = D^4 - d^4$	[e]DL coefficients	
(in)	(mm)	(mm)	(mm)	(mm)	(kN)	(mm)	(kN/mm)	(kN)	(mm)	(kN/mm)					D/(L.D)	D/L^3
0.5	21.3	3.73	13.84	170	10.9	1.9	5.7	21.7	9.3	1.45	2.0	0.011	0.25	169,145	46.7	0.0344
				188	9.7	2.0	4.9	20.4	10.3	1.28	2.1	0.011	0.26		42.2	0.0255
				210	8.1	2.1	4.0	19.2	11.5	1.17	2.4	0.010	0.30		37.8	0.0183
				230	7.3	2.2	3.4	17.8	12.6	1.00	2.4	0.009	0.30		34.5	0.0139
				250	6.4	2.3	2.8	16.6	13.7	0.89	2.6	0.009	0.31		31.8	0.0108
0.75	26.7	3.8	19.1	170	18.2	1.9	9.8	35.1	9.3	2.26	1.9	0.011	0.23	375,126	82.6	0.0764
				188	16.9	2.0	8.4	33.3	10.3	1.97	2.0	0.011	0.23		74.7	0.0565
				210	14.4	2.0	7.2	31.2	11.5	1.76	2.2	0.010	0.25		66.9	0.0405
				230	12.9	2.1	6.2	28.7	12.6	1.49	2.2	0.009	0.24		61.1	0.0308
				250	11.7	2.2	5.3	26.7	13.7	1.30	2.3	0.009	0.24		56.2	0.0240
1	33.4	4.55	24.3	170	32.7	1.9	17.6	63.8	9.3	4.15	2.0	0.011	0.24	895,796	157.8	0.1823
				188	30.5	2.0	15.2	59.8	10.3	3.52	2.0	0.011	0.23		142.7	0.1348
				210	25.8	2.0	13.2	56.1	11.5	3.16	2.2	0.009	0.24		127.7	0.0967
				230	24.4	2.1	11.6	52.0	12.6	2.61	2.1	0.009	0.22		116.6	0.0736
				250	22.7	2.2	10.3	48.6	13.7	2.24	2.1	0.009	0.22		107.3	0.0573
1 1/4	42.2	4.85	32.5	170	46.7	1.9	25.2	96.5	9.3	6.64	2.1	0.011	0.26	2,055,727	286.6	0.4184
				188	44.7	1.9	23.5	94.7	10.3	5.92	2.1	0.010	0.25		259.1	0.3094
				210	41.5	2.0	21.3	89.6	11.5	5.01	2.2	0.009	0.24		232.0	0.2220
				230	40.1	2.1	19.6	84.4	12.6	4.18	2.1	0.009	0.21		211.8	0.1690
				250	38.5	2.2	17.9	79.6	13.7	3.54	2.1	0.009	0.20		194.9	0.1316
1 1/2	48.3	5.08	38.14	170	50.5	1.8	28.1	109.0	9.3	7.75	2.2	0.011	0.28	3,326,341	405.1	0.6770
				188	53.3	1.9	28.0	109.0	10.3	6.61	2.0	0.010	0.24		366.3	0.5006
				210	50.1	2.0	25.7	107.0	11.5	5.93	2.1	0.009	0.23		327.9	0.3592
				230	49.9	2.1	24.3	103.7	12.6	5.08	2.1	0.009	0.21		299.4	0.2734
				250	48.9	2.2	22.8	99.7	13.7	4.38	2.0	0.009	0.19		275.5	0.2129

[a] Thickness.
[b] Inside Diameter (d = D-2 t).
[c] Target Displacement ($D_u = 0.055 \times L$).
[d] Auxiliary parameter
[e] DL coefficient consists of pipe Diameter (D) and Length (L).

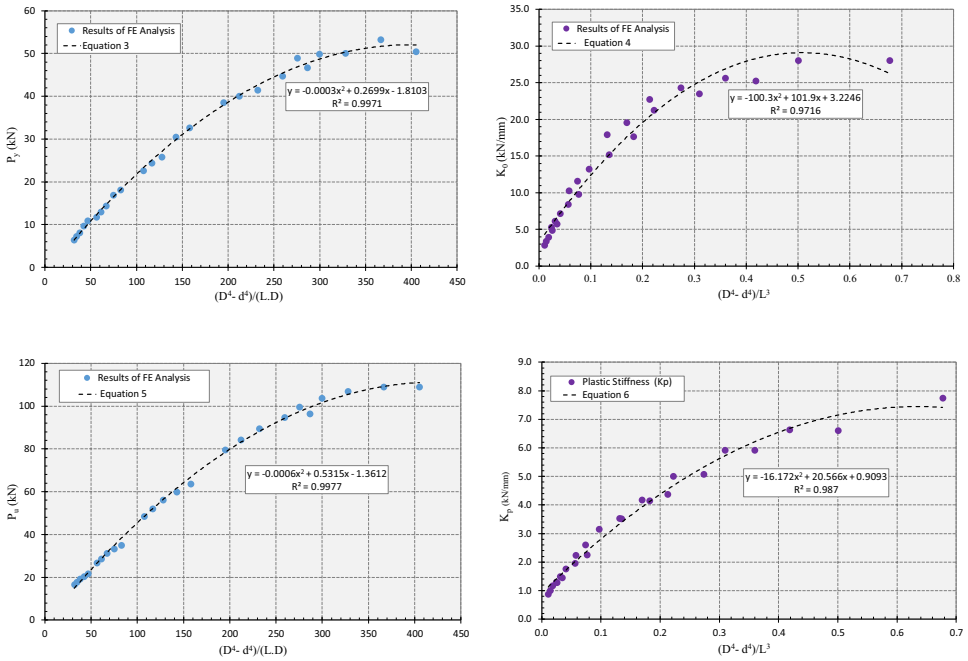

Fig. 11. Mechanical properties vs. relevant LD coefficients.

in terms of the pipe's internal and external diameters (d and D) and the pipe's length (L): $P \propto \frac{(D^4-d^4)}{(L.D)}$ and $K \propto \frac{(D^4-d^4)}{L^3}$. These DL coefficients for different numerically tested PFDs were calculated and listed in Table 5.

The four obtained factors from the numerical study, i.e. the yield and ultimate strengths; the primary and secondary stiffness, versus their corresponding DL coefficient are plotted in Fig. 11. Besides, a proper trendline and its equation for the mention variables are suggested in the figure. As can be seen, the suggested equations are of the second-order type with an accuracy of over 96%.

After applying the number of bars (N) in the obtained equations, the formulas proposed for the strength and stiffness of the PFD are as follows. In these formulas, the units of length and diameter are in millimetres and the units of strength and stiffness are in kN and kN/mm, respectively. The given formulas show that the pipe thickness is directly related with the strength and stiffness of the proposed damper, whereas these properties are inversely proportional to the pipe length.

$$P_y = N\left(-.0003\left[\frac{\left(D^4-d^4\right)}{L.D}\right]^2 + .27\left[\frac{\left(D^4-d^4\right)}{L.D}\right] - 1.81\right) \quad (3)$$

$$K_0 = N\left(-100\left[\frac{\left(D^4-d^4\right)}{L^3}\right]^2 + 102\left[\frac{\left(D^4-d^4\right)}{L^3}\right] + 3.22\right) \quad (4)$$

$$P_u = N\left(-.0006\left[\frac{\left(D^4-d^4\right)}{L.D}\right]^2 + .53\left[\frac{\left(D^4-d^4\right)}{L.D}\right] - 1.36\right) \quad (5)$$

$$K_p = N\left(-16.2\left[\frac{\left(D^4-d^4\right)}{L^3}\right]^2 + 20.6\left[\frac{\left(D^4-d^4\right)}{L^3}\right] + .91\right) \quad (6)$$

Regarding the proposed formula (Eq. 5) for the ultimate strength of the damper and having the geometry specification for five standard pipes, a design chart was developed for the strength of one pipe with different lengths of these standard pipes, as shown in Fig. 12. For example, if a PFD is added to a brace with a total capacity of 250 kN, this design chart will be used as follows. The final strength of 50 kN is obtained for each pipe while assuming 5 fuses for this damper, where its appropriate length and diameter can be determined according to the presented chart. In this example, with respect to the ultimate strength of 50 kN in the vertical axis, a pipe with diameter and thickness of 33 and 4.5 mm, respectively, and a length of 250 mm, can be selected from the curve and horizontal axis, respectively.

5. Pipe-Fuse Damper (PFD) vs. Bar-Fuse Damper (BFD)

Since simple steel bar was previously studied in the Fuse Damper [13], some behaviours of the BFD and PFD are compared in this section. For this purpose, the results of specimens 1Bar14 and 1Pipe21(3), which have fuses with almost equal length and cross-sectional area, were selected to study their performance under different tests. To undertake a comprehensive comparison, the results of tensile tests on the used pipe and bar in the dampers are shown in Fig. 13(a). As can be seen, both parts have similar elasticity modules and close ultimate strength, whereas the pipe has a yield strength almost 40% less than the bar. Based on the obtained elongation at failure points for the both

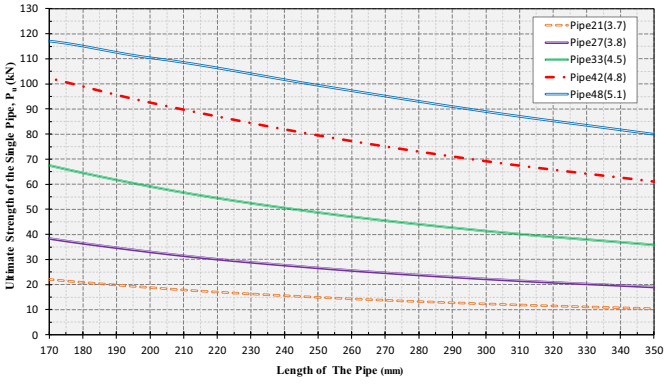

Fig. 12. Design curves for Pipe-Fuse Damper (PFD).

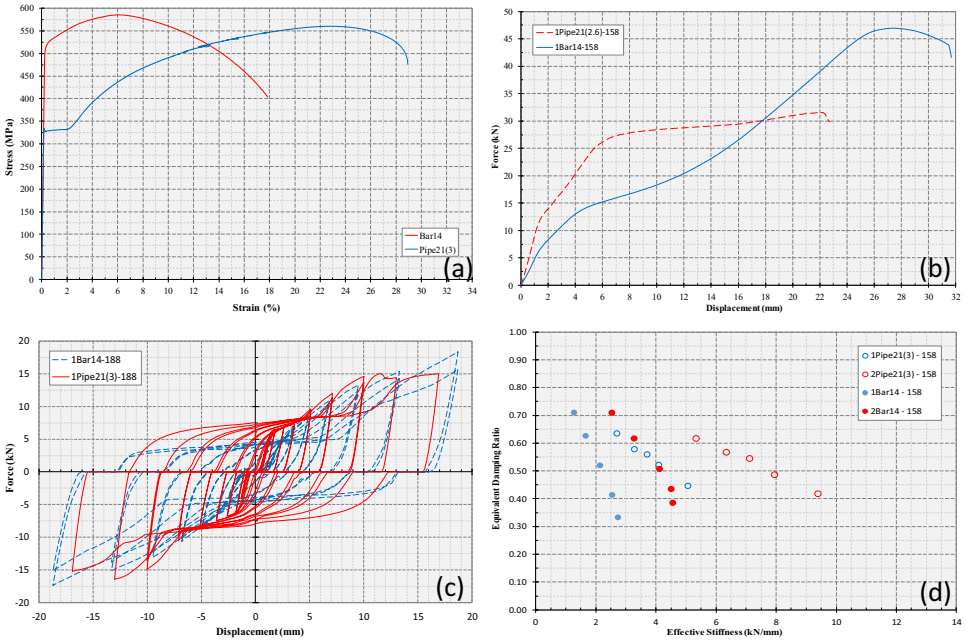

Fig. 13. BFD vs. PFD: a) tensile tests for bar and pipe, b) monotonic tests, c) cyclic tests, d) damping ratio and effective stiffness.

components, it can be claimed that the material of the used pipes had a higher ductility compared to the bar material.

Fig. 13(b) shows the results of conducted monotonic tests for two specimens of 1Bar14-158 and 1Pipe21(3)-158. These two dampers are completely identical in terms of geometric characteristics, except for the shape of cross-sections in the applied fuses. Therefore, the dissimilar behaviour of the specimens under the similar experiments can be attributed to the different shape of fuses in the PFD and BFD. In terms of the stiffness, the pipe had higher stiffness than the bar within 6 mm of initial displacement. From the mentioned point to the failure, the pipe stiffness remains almost constant, whereas the bar showed an increasing stiffness in this range. Regarding the ultimate strength, the bar had much more strength than the pipe. Also, both members were roughly yielded at the same yield displacement, whereas the yield strength for the pipe is almost twice of the bar. In terms of energy dissipation of sacrificial elements in the Fuse Damper (FD), it can be said that the pure plastic behaviour of the pipe in the PFD is preferable, rather than the hardening behaviour of the bar in the BFD.

Fig. 3(c) shows the force-displacement hysteresis of two specimens 1Bar14-188(BFD) and 2Pipe21(3)-188(PFD) obtained from the cyclic tests under same conditions. Regarding strength and initial stiffness, the PFD has a bigger value than the BFD in most load cycles. Importantly, the PFD shows fewer pinching effects in its response to a great extend compared to the BFD. Furthermore, considering the area of loops in both hysteresis, the PFD dissipates a higher amount of energy than the BFD in the same displacement domain.

The variations of effective stiffness versus the equivalent damping ratio of the PFD and BFD are shown in Fig. 13(d). As can be seen, the effective stiffness of dampers with the pipes is higher than that of the dampers with the bars. The bars have a wider range and higher maximum than the pipe in terms of the equivalent damping ratio, although both have almost equal average value. Likewise, it is seen that the damping ratio of the BFD rises more rapidly than PFD by increasing the displacement.

6. Conclusions

In this paper, the steel pipes were used as energy absorber elements in the fuse part of Fuse Damper (FD). The Pipe-Fuse Damper (PFD) was individually examined as a new passive damper through practical experiments and numerical analyses. A series of cyclic and monotonic tests performed and showed that the Pipe-Fuse Damper (PFD) is capable of dissipating energy with the stable hysteretic behaviour in the specific displacement domain without a sudden deterioration in the stiffness and strength. The main findings of this study are summarized as follows:

1. The steel pipes as fuses and energy-absorbing elements can control the mechanical property of the FD with four geometric parameters, including the number, length, diameter and thickness of the pipes. Theses parameters are easily able to suit any requirements needed for the FD as a metallic damper.
2. To have a reliable performance, it is suggested that the target displacement of the PFD to be selected less than the 5.5% of the bending length of the pipes. This selection can guarantee at least 20 load cycles defined by FEMA461 without any considerable degradation in the stiffness and strength of the damper.
3. In general, the PFD can provide an equivalent viscous damping ratio and equivalent stiffness in range of 25–80% and 1.5–10 kN/mm, respectively. On average, the unit weight of employed steel pipes sustained 41 kN force and dissipated 9 kJ of input energy. Moreover, the damping ratio of the PFD is inversely correlated to the pipe diameters when the pipe thicknesses are the same.
4. Based on the obtained results, the steel pipes can give a hysteric behaviour with less pinching effect to the FD relative to the steel bars. Besides, the PFD dissipates energy higher than the BFD in the same domain of displacement.

The results of this experimental study show that the Pipe-Fuse Damper (PFD) has the capability to be used as an energy dissipating device for seismic upgrading of the structures. It should be noted that the presented work is a feasibility study and some further investigations are required before applying the proposed damper to real structures.

Acknowledgment

The work reported in this study was graciously supported by Research University Grant Scheme (RUGS) under Universiti Teknologi Malaysia with grant number Q.J130000.2509.14H28. The authors remain indebted for the support given by them.

References

[1] M.D. Symans, A.M. Asce, F.A. Charney, F. Asce, A.S. Whittaker, M. Asce, M.C. Constantinou, C.A. Kircher, M.W. Johnson, R.J. Mcnamara, Energy dissipation systems for seismic applications: current practice and recent developments, J. Struct. Eng. 134 (2008) 3–21, https://doi.org/10.1061/ASCE0733-94452008134:13.

[2] K. Muto, Earthquake resistant design of 36-storied Kasumigaseki building, Proc. 4th World Conf. Earthq. Eng. 3 1969, pp. 16–33http://www.mendeley.com.

[3] J. Guerrero, Bandas amortiguadoras para muros de particio'n (damping strips for partition walls), Memorias Del Prim. Congr. Nac. Ing. Sı'smica, Spanish 1965, pp. 75–85.

[4] J.M. Kelly, R.I. Skinner, A.J. Heine, Mechanisms of energy absorption in special devices for use in earthquake resistant structures, Bull. NZ Soc. Earthq. Eng. 5 (1972) 63–88.

[5] R.I. Skinner, J.M. Kelly, A.J. Heine, Hysteretic dampers for earthquake-resistant structures, Earthq. Eng. Struct. Dyn. 3 (1975) 287–296, https://doi.org/10.1002/eqe.4290030307.

[6] K. Tsai, Huan-Wei Chen, Ching-Ping Hong, Su Yung-Feng, Design of steel triangular plate energy absorbers for seismic-resistant construction, Earthquake Spectra 9 (1993) 505–528, https://doi.org/10.1193/1.1585727.

[7] R.W.K. Chan, F. Albermani, Experimental study of steel slit damper for passive energy dissipation, Eng. Struct. 30 (2008) 1058–1066, https://doi.org/10.1016/j.engstruct.2007.07.005.

[8] M.G. Gray, C. Christopoulos, J.A. Packer, Cast steel yielding fuse for concentrically braced frames, 9th US Natl. 10th Can. Conf. Earthq., Torento, Ontario, Canada 2010, pp. 4235–4244.

[9] A. Salem Milani, M. Dicleli, Systematic development of a new hysteretic damper based on torsional yielding: part I—design and development, Earthq. Eng. Struct. Dyn. 45 (2016) 845–867, https://doi.org/10.1002/eqe.

[10] J. Lee, J. Kim, Development of box-shaped steel slit dampers for seismic retrofit of building structures, Eng. Struct. 150 (2017) 934–946, https://doi.org/10.1016/j.engstruct.2017.07.082.

[11] M. Rezai, H. Prion, R. Tremblay, Seismic performance of brace fuse elements for concentrically steel braced frames, STESSA 2000 Conf, Montreal, Canada 2000, pp. 39–46.

[12] R. Tremblay, et al., Overview of ductile seismic brace fuse systems in Canada, EuroSteel 2011, Budapest, Hungary 2011, pp. 939–944.

[13] R. Aghlara, M.M. Tahir, A passive metallic damper with replaceable steel bar components for earthquake protection of structures, Eng. Struct. 159 (2018) 185–197, https://doi.org/10.1016/j.engstruct.2017.12.049.

[14] S. Maleki, S. Mahjoubi, Infilled-pipe damper, J. Constr. Steel Res. 98 (2014) 45–58, https://doi.org/10.1016/j.jcsr.2014.02.015.

[15] F. Casciati, M. Domaneschi, Semi-active electro-inductive devices: characterization and modelling, J. Vib. Control. 13 (2007) 815–838, https://doi.org/10.1177/1077546307077465.

[16] M. Ismail, J. Rodellar, G. Carusone, M. Domaneschi, L. Martinelli, Characterization, modeling and assessment of Roll-N-Cage isolator using the cable-stayed bridge benchmark, Acta Mech. 224 (2013) 525–547, https://doi.org/10.1007/s00707-012-0771-4.

[17] G. De Mari, M. Domaneschi, M. Ismail, L. Martinelli, J. Rodellar, Reduced-order coupled bidirectional modeling of the Roll-N-Cage isolator with application to the updated bridge benchmark, Acta Mech. 226 (2015) 3533–3553, https://doi.org/10.1007/s00707-015-1394-3.

[18] S. Maleki, S. Bagheri, Pipe damper, part I: experimental and analytical study, J. Constr. Steel Res. 66 (2010) 1088–1095, https://doi.org/10.1016/j.jcsr.2010.03.010.

[19] S. Maleki, S. Mahjoubi, Dual-pipe damper, J. Constr. Steel Res. 85 (2013) 81–91, https://doi.org/10.1016/j.jcsr.2013.03.004.

[20] R.W.K. Chan, F. Albermani, S. Kitipornchai, Experimental study of perforated yielding shear panel device for passive energy dissipation, J. Constr. Steel Res. 65 (2009) 260–268, https://doi.org/10.1016/j.jcsr.2013.08.013.

[21] ASTM Int., ASTM A370, Test Methods for Tension Testing of Metallic Materials 1, Astm. i, 2009 1–27, https://doi.org/10.1520/E0008.

[22] FEMA 461. Federal Emergency Management Agency, Testing Protocols for Determining the Seismic Performance Characteristics of Structural and Nonstructural, 2007 (Washington, DC).

[23] R. Aghlara, M.Md. Tahir, A. Adnan, Comparative study of eight metallic yielding dampers, J. Teknol. 77 (2015) 119–125, https://doi.org/10.11113/jt.v77.6408.